

## Critical Exponents of Gelation and Conductivity in Polyacrylamide Gels Doped by Multiwalled Carbon Nanotubes

Demet Kaya Aktaş , Gülşen Akin Evingür & Önder Pekcan

To cite this article: Demet Kaya Aktaş , Gülşen Akin Evingür & Önder Pekcan (2010) Critical Exponents of Gelation and Conductivity in Polyacrylamide Gels Doped by Multiwalled Carbon Nanotubes, Composite Interfaces, 17:4, 301-318, DOI: [10.1163/092764410X495243](https://doi.org/10.1163/092764410X495243)

To link to this article: <https://doi.org/10.1163/092764410X495243>



Published online: 02 Apr 2012.



Submit your article to this journal [↗](#)



Article views: 62



View related articles [↗](#)



Citing articles: 15 View citing articles [↗](#)

# Critical Exponents of Gelation and Conductivity in Polyacrylamide Gels Doped by Multiwalled Carbon Nanotubes

Demet Kaya Aktaş<sup>a</sup>, Gülşen Akin Evingür<sup>a</sup> and Önder Pekcan<sup>b,\*</sup>

<sup>a</sup> Istanbul Technical University, 34469 Maslak-Istanbul, Turkey

<sup>b</sup> Kadir Has University, 34320 Cibali-Istanbul, Turkey

Received 29 December 2008; accepted 9 March 2009

## Abstract

Polyacrylamide (PAM) doped by multiwalled carbon nanotube (MWNT) gels were prepared with different amounts of MWNTs varying in the range between 0.1 and 15 wt%. The PAM–MWNT composite gels were characterized by the steady state fluorescence technique (SSF). The alternative electrical conductivity (AC) of PAM–MWNT composite gels was measured by the dielectric spectroscopy technique. Observations around the gel point,  $t_{gel}$  for PAM–MWNTs composite gels showed that the gel fraction exponent  $\beta$  obeyed the percolation result. The critical exponent  $r$  of AC electrical conductivity for the composite PAM–MWNT gel was also measured and found to be about 2.0, which agrees with a random resistor network.

© Koninklijke Brill NV, Leiden, 2010

## Keywords

Acrylamide, multiwalled carbon nanotubes, hydrogel, percolation, critical phenomena, fluorescence

## 1. Introduction

Since the discovery of carbon nanotubes (CNTs) in 1991 by Lijima [1], single-wall carbon nanotubes (SWNT) and multiwalled carbon nanotubes (MWNT) have attracted great interest throughout the academic world, as well as being utilized in industrial applications [2]. Because of their high mechanical strength, high aspect ratio, small diameter, light weight, high electrical and thermal conductivities, and high thermal and air stabilities, many applications in the industrial world have been found for CNTs [3]. Moreover, polymer composites with carbon nanotube additions are one of the research subjects which have attracted a lot of attention in recent years [4, 5]. The first polymer nanocomposites using carbon nanotubes as filler were reported in 1994 by Ajayan *et al.* [6]. In earlier nanocomposites, nanoscale fillers were

\* To whom correspondence should be addressed. E-mail: pekcan@khas.edu.tr

used such as carbon blacks, silica, clays, and carbon nanofibers (CNF) to improve the mechanical, electrical, and thermal properties of polymers. In recent years, carbon nanotubes have been used to improve the electrical and mechanical properties of polymers [7–12]. However, due to the advantage provided by the surface morphology, the literature has focused on polymer composite thin films [13–19], while there are no detailed studies on tri-dimensional composite gels with carbon nanotube content.

Gels appear during a random linking process of monomers to larger and larger molecules. Even though the sol–gel transition is not a phase transition in the thermodynamic sense (as it is a geometrical one), as a subject of critical phenomenon, it behaves like a second order phase transition and constitutes a universal class by itself [20]. Experimental techniques used for monitoring sol–gel transition must be very sensitive to structural changes, and should not disturb the system mechanically. The fluorescence technique is particularly useful for the elucidation of the detailed structural aspects of the gels. This technique is based on the interpretation of the change in anisotropy, emission and/or excitation spectra, emission intensity, and viewing the lifetimes of injected aromatic molecules to monitor the change in their microenvironment [21–24].

Electrical measurements are an unambiguous criterion of the existence of a percolated network in the case of conductive fillers in an isolating matrix. Dielectric measurements performed with varying frequency can lead to additional information about the percolation network, as has been shown for percolation structures of carbon black in polymeric matrices. Recently, results on percolated structures of carbon nanotubes in disc sheet dry gels were presented [25]. Similarly, the AC and DC conductivities of carbon nanotubes–polyepoxy composites have been investigated from 20° to 110°C in the frequency range  $10^{-2}$ – $10^6$  Hz as a function of the conductive weight fraction, ranging from 0.04 to 2.5 wt% [26]. The ability of existing theories to predict electrical properties of conductive fiber composites has been examined [27]. Complex permittivity and related AC conductivity measurements in the frequency range between  $10^{-4}$ – $10^7$  Hz are presented for composites of polycarbonates (PCs) filled with different amounts of multiwalled carbon nanotubes (MWNTs) varying in the range between 0.5 and 5 wt% [28]. In addition, the conductivity of dry gel composites such as polystyrene [3] and polypropylene [29] has been enhanced significantly with the addition of CNTs. On the other hand, the PAM–CNT composite thin films were characterized by the instruments of Fourier transform infrared spectroscopy, UV–VIS absorbance spectra, fluorescence spectra and transmission electron microscope [30]. Dielectric spectroscopy represents a method which has been successfully applied to investigate the percolation structure of CNTs in polymer (see, e.g., [2, 3, 29]). Therefore, we expect that this method can lead to new insights in MWNT-doped systems.

The main goals of this work include analysis of the influence of MWNTs' dispersion on gelation (occurring in composite gels) and the conductivity properties of composites. In this study, composite gel systems (which are initially of isolator

character) are produced by the inclusion of carbon nanotubes, which are capable of converting the system into electrically conductive structure when the amount of the addition exceeds a critical value known as the percolation threshold. At this point, the composite gels are analyzed using the steady state fluorescence and dielectric spectroscopy, where the total monomer concentration is kept at 2 M and a very small amount of pyranine ( $10^{-4}$  M) is added to the pre-polymerization solution. The spectral shift to shorter wavelengths is observed due to the binding of pyranine to the polymer chains during the formation of PAM–MWNT composite gels. The pyranine then becomes an intrinsic fluoroprobe while it is extrinsic at the beginning of the reaction. The fluorescence intensity of the pyranine bonded to the strands of the polymers allows one to measure directly the gel fraction near the sol–gel phase transition point, and thus the corresponding critical exponent  $\beta$ , which is found to be in close agreement with the percolation model.

The percolation structure of conductivity and the state of dispersion of MWNTs in polyacrylamide gels are also investigated using dielectric spectroscopy. Here the critical conductivity exponent, around the conductivity percolation threshold where a material shifts to a conductor from a character of insulation, is determined and found to be about 2.0, in agreement with a random resistor network.

## 2. Background

### 2.1. Percolation Theory for Gelation

Several theories have been developed in the past half century to describe gel formation, among which the Flory–Stockmayer theory and percolation theory have provided the bases for modeling the sol–gel phase transition [31–37]. Statistical theories based on a tree-like structure (Bethe lattice) use a mean field approximation, which originates from Flory [31] and Stockmayer [32], and assume equal reactivities of functional groups and the absence of cyclization reactions. Most statistical theories derived in the following decades are fully equivalent, differing only in mathematical language [38–41]. Percolation offers a particularly simple and yet detailed picture through which one may seek to understand gelation [33–35, 37]. In the language of percolation, one may think of monomers as occupying the vertices of a periodic lattice, and the chemical bonds as corresponding to the edges joining these vertices, at any given moment, with some probability  $p$ . Then, the gel point can be identified with the percolation threshold  $p_c$ , where, in the thermodynamic limit, the incipient infinite cluster starts to form. Identifying the weight average degree of polymerization  $DP_w$  with the average cluster size  $S_{av}$  and the gel fraction  $G$  with the probability  $P_\infty$  of an occupied site belonging to the incipient infinite cluster, one can predict the scaling behavior of these and related quantities near the gel point, as a function of  $|p - p_c|$ ,

$$DP_w \propto (p_c - p)^{-\gamma}, \quad p \rightarrow p_c^-, \quad (1)$$

$$G \propto (p - p_c)^\beta, \quad p \rightarrow p_c^+. \quad (2)$$

If  $p$  approaches  $p_c$  from below it is denoted as  $p \rightarrow p_c^-$ ; in contrast,  $p \rightarrow p_c^+$  denotes when  $p$  approaches  $p_c$  from above. Here,  $\beta$  and  $\gamma$  are the critical exponents and  $A$  and  $B$  are the proportionality factors. The critical exponents in percolation theory,  $\beta = 0.41$  and  $\gamma = 1.80$ , differ from those found in Flory–Stockmayer, where  $\beta = 1$  and  $\gamma = 1$ .

## 2.2. Percolation Theory of Conductivity

The percolation theory has been used to interpret behavior in a mixture of conducting and non-conducting components [27]. Schematic representation of the electrical percolation threshold (before and after) is shown in Fig. 1(a) and 1(b). Direct connection and overlapping of the CNT is not necessary; i.e., nanotubes do not need to physically touch each other for conductivity. Nanotubes can just be close enough to allow for a hopping/tunneling electron effect; these mechanisms require the CNT–CNT distance to be less than 5 nm. As a result, a higher volume fraction of CNT's filler is needed to achieve the electrical percolation threshold [2]. Two classes of models have been developed for the description of the frequency dependence of the complex conductivity:

$$\sigma^*(w) = \sigma'(w) - i\sigma''(w), \quad (3)$$

where  $\sigma'(w)$  forms the real part, and  $\sigma''(w)$  the imaginary part of the complex conductivity,  $i$  the imaginary unit, and  $w$ , the angular frequency in the percolating systems:

(i) The equivalent circuit model, which treats a percolation system as a random mixture of resistors and capacitors [37, 42], and (ii) the model based on charge carrier diffusion on percolating clusters [37, 43]. For two-component systems, a percolation cluster of high conductivity ( $\sigma_1$ ) embedded in a matrix of considerable lower conductivity ( $\sigma_2, \sigma_2 \ll \sigma_1$ ) — macroscopic effective conductivity near the percolation threshold  $p_c$  can be written in the scaling form [37, 42, 44]:

$$\sigma(p, w) \propto \sigma_1 |p' - p'_c|^r \Phi_{\pm} \left( \frac{\sigma_2}{\sigma_1} |p' - p'_c|^{-(r+s)} \right), \quad (4)$$

where  $p'$  is the concentration of conducting filler,  $\Phi_+$  and  $\Phi_-$  denote scaling functions for  $p' > p'_c$  and  $p' < p'_c$ , respectively, and  $s$  and  $r$  are the critical exponents. These models treat a percolation system as a random mixture of resistors,  $R$ , and capacitors,  $C$ , having a characteristic relaxation time  $\tau = \frac{1}{\omega_0} = RC$ , where scaling law equation (4) for the complex conductivity near the percolation threshold takes the following form [37, 42, 44]:

$$\sigma^*(p, w) \propto \frac{1}{R} |p' - p'_c|^r \Phi_{\pm} \left( \frac{iw}{\omega_0} |p' - p'_c|^{-(r+s)} \right). \quad (5)$$

One of the main physical contents of this key scaling law is the existence of a time scale:

$$\tau_c(p') \propto \frac{1}{\omega_p(p')} \propto \frac{1}{\omega_0} |p' - p'_c|^{-(r+s)}, \quad (6)$$

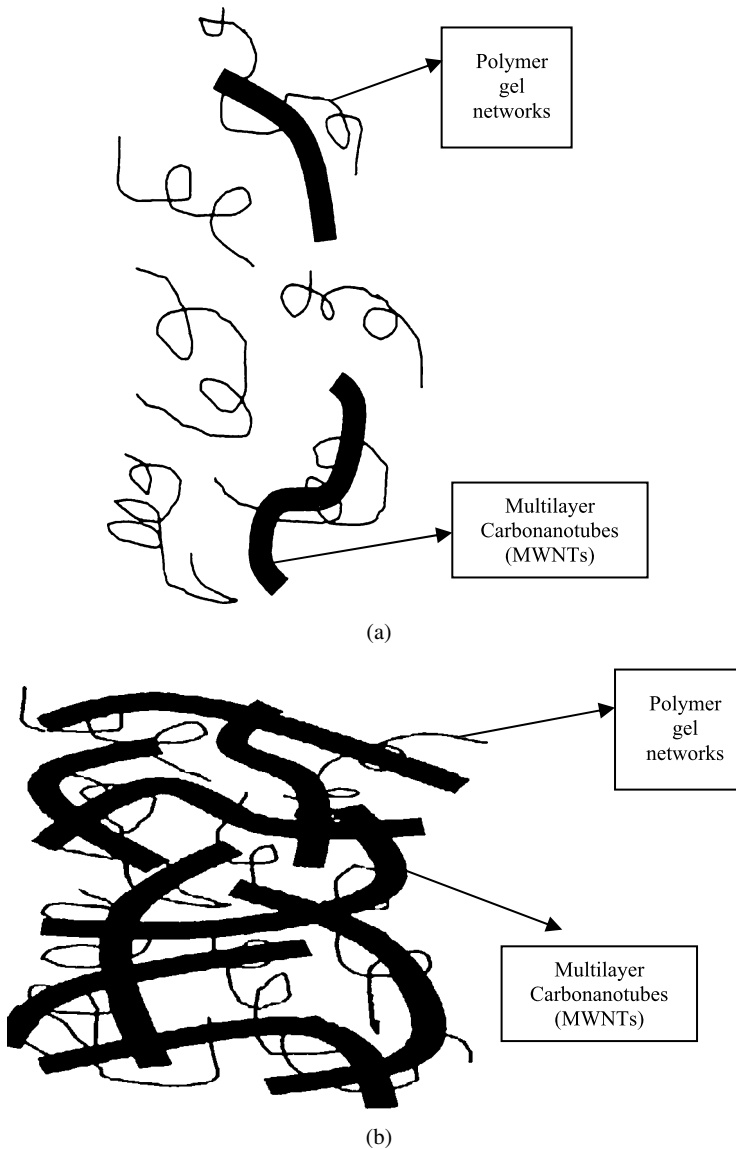


**Figure 1.** Schematic of CNTs/polymer composite with isotropic orientation of nanotubes (a) before and (b) after formation of electrical percolation threshold.

that diverges as the percolation threshold is approached from both sides.

For the frequency dependence of AC conductivity at the percolation threshold, Bergman and Imry [42] have derived the following law:

$$\sigma'(w) \propto w^{\frac{r}{r+s}}, \quad (7)$$

where  $\sigma'$  is the real part of equation (3);  $w$ , the angular frequency; and  $r$  and  $s$  critical exponents for conductivity. A wide variety of approaches have been ap-

**Table 1.**

Critical exponents for electrical percolation threshold in three dimensions (3D)

System	$r$	$s$	References
Resistor lattice	$1.70 \pm 0.05$	$0.70 \pm 0.05$	Straley [44]
Random resistor network	$1.95 \pm 0.03$	–	Fisch and Harris [45]
Random resistor network	$2.02 \pm 0.05$	–	Adler <i>et al.</i> [46]
Random resistor lattices	$2.003 \pm 0.047$	–	Gingold and Lobb [47]
Random resistor network	$1.9 \pm 0.1$	$0.75 \pm 0.04$	Herrman <i>et al.</i> [48], Derrida <i>et al.</i> [49]

plied to the determination of these exponents as given in Table 1 for 3D with Refs [44–49].

### 3. Experimental

We used MWNT that was analyzed by the Delta Nu Advantage 532 Raman Spectrometer with 100–3400 wave number spectral range (Cheap Tubes Inc., USA) with a length of 20–30 nm and a diameter of 10–30  $\mu\text{m}$ . The purity of the MWNT was >95 wt%.

Initially, the solution is composed of MWNTs, PVP and water, in the proportions of 10 parts MWNTs: 1–2 parts PVP:2000 parts distilled water at room temperature. The required dispersion time is approximately 5 or 6 min with an interruption of 10 s, every 30 s at full or high amplitude by using ALEX ultrasonic equipment.

Composite gels were prepared by using 2 M AAm (acrylamide, Merck) with various amounts (0.1–15 wt%) of MWNTs stock concentration at room temperature. AAm, the linear component; BIS (N,N'-methylenebisacrylamide, Merck), the initiator; and TEMED (tetramethylethylenediamine, Merck), and the accelerator were dissolved in distilled water. The initiator and pyranine concentrations were kept constant at  $7 \times 10^{-3}$  M and  $4 \times 10^{-4}$  M, respectively, for all samples. After bubbling nitrogen for 10 min, each pre-composite gel solution of 5 ml was poured into a cylindrical glass tube and put into the sample holder of the spectrometer.

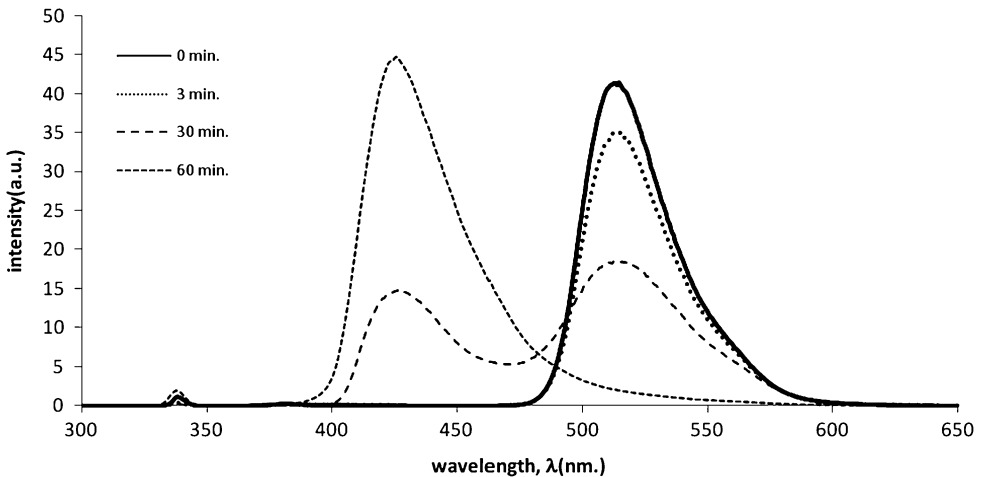
The fluorescence intensity measurements during gelation were carried out using the Model LS-50 spectrometer by Perkin-Elmer. All measurements were made at a 90° position and slit widths were kept at 2.5 nm. Pyranine was excited at 340 nm wavelength of light and variation in the fluorescence spectra and emission intensity of the pyranine were monitored as a function of gelation time.

AC dielectric spectroscopy was performed with a dielectric spectrometer HP-4192 A impedance analyzer controlling a computer. Samples with a diameter of 14 mm and thicknesses ranging from 1–2 mm were placed in the holder between two parallel stainless steel-plated electrodes (14 mm in diameter). All experiments were carried out at a constant temperature of 25°C. Conductivity was measured and plotted as a function of the frequency.

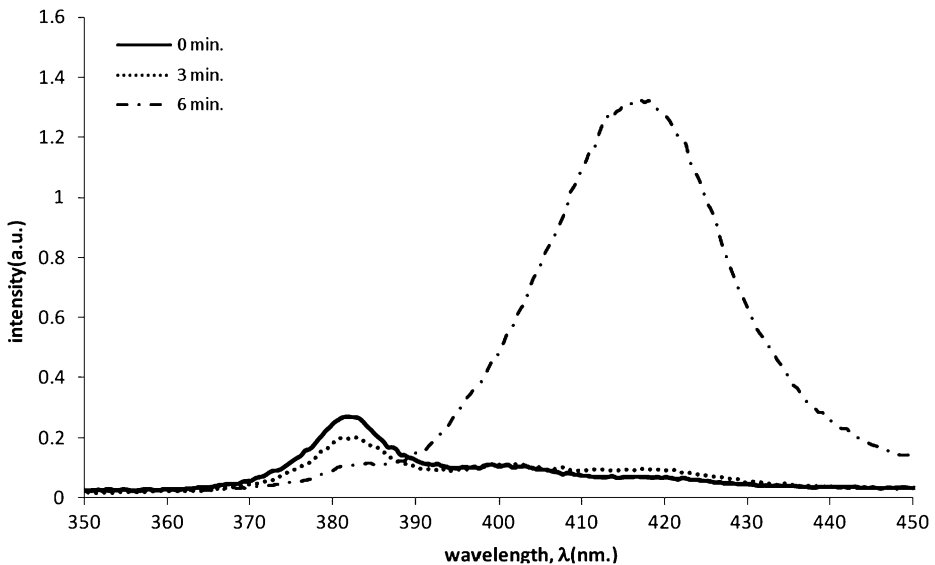
## 4. Results and Discussion

### 4.1. Gelation Exponents

The typical fluorescence spectra of pyranine recorded at different stages of gelation of PAM–MWNT composites are shown in Fig. 2. As seen in Fig. 2(a), at the beginning of the reaction, only the 512 nm peak exists, and then the intensity of the new (short-wavelength) peak around 380 nm (see Fig. 2(b)) starts to increase



(a)



(b)

**Figure 2.** Typical fluorescence spectra of pyranine at different stages of gelation for PAM–MWNTs composite (a) during the whole course of gelation presenting the binding of pyranines, (b) at the early stage of gelation, presenting the spectral shift from 380 nm toward 427 nm.

as the intensity of the 512 nm peak (long-wavelength) decreases during the course of gelation of PAM–MWNT composite gels. The increase in 380 nm emission is due to a C–O ether bond formation between the hydroxylic oxygen of 3sPyOH and a terminal C-atom of the growing AAm chain [51]. Meanwhile, as the polymerization progresses, the maxima of the short wavelength-peak shift to some higher wavelengths, starting from 380 nm and ending at 427 nm, as presented in Fig. 2(a) and 2(b) [50]. The shift in the short-wavelength region between 380 nm and 427 nm is probably due to the complexation of  $\text{SO}_3^-$  groups with protonated amide groups, whether on the same polymer molecule or on the other polymer strands [51]. The reason for the shift in the isoemissive (isostilbic) point is the change in the internal morphology of the system: at the beginning of the polymerization the system is in the ‘sol’ state (all pyranine are free) and above a certain time it turns into the ‘gel’ state (most of the pyranine are bonded).

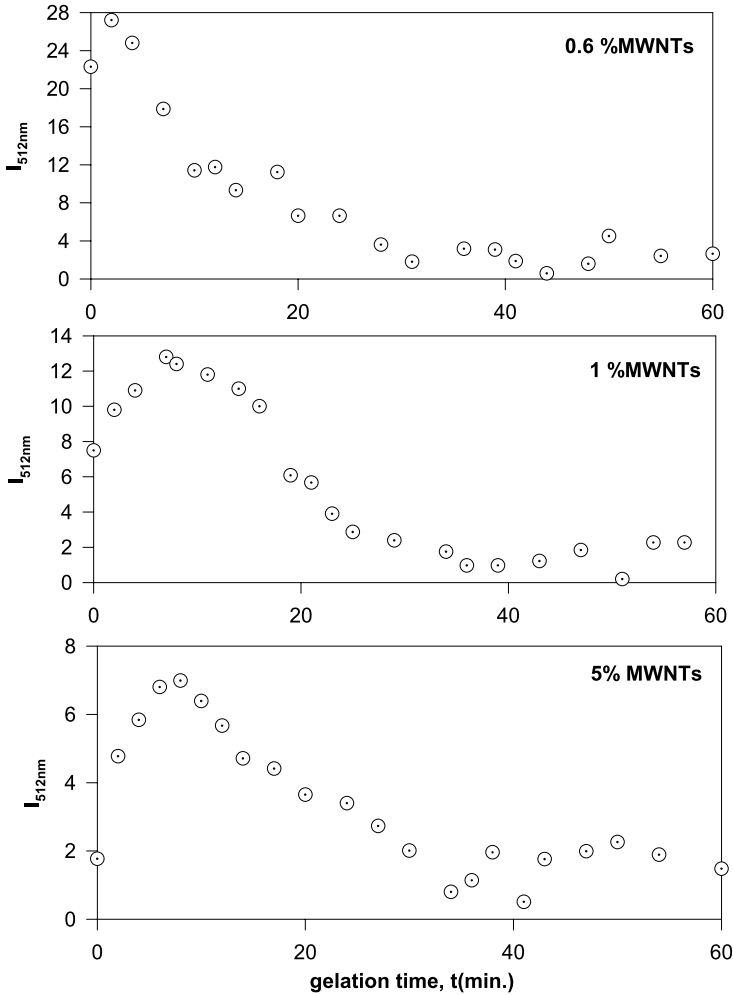
Figure 3 presents the fluorescence intensity,  $I_{512 \text{ nm}}$  of the free pyranine (512 nm) from the reaction mixture as a function of the gelation time for 0.6, 1 and 5% MWNT concentrations. As seen in Fig. 3, the fluorescence intensity increased up to some point (gelation stage), and then decreased to zero at the end of the reaction (final stage) for different MWNT concentrations.

Figure 4 shows the fluorescence intensities,  $I_{\text{em}}$ , from the bonded pyranine (427 nm) against the gelation time for 0.6, 1 and 5% MWNT concentrations. Since the maxima of the spectra shift from 380 nm to 427 nm as the gelation progresses, we monitored the fluorescence spectra in relatively large periods of time and plotted the intensity  $I_{\text{em}}$  corresponding to the maxima of the spectra as a function of time. These data were used to evaluate the critical behavior of the sol–gel phase transition [50].

In order to determine the gel points,  $t_{\text{gel}}$ , each experiment was repeated in the same experimental conditions, and the gel points were determined by the dilatometric technique [52]. A steel sphere of 4.8 mm diameter was moved in the sample up and down slowly by means of a magnet applied from the outer face of the sample cell. The time at which the motion of the sphere is stopped is called the onset of the gel point,  $t_{\text{gel}}$ . The  $t_{\text{gel}}$  values are summarized in Table 2, together with the other parameters.

Here, one would like to argue that the total fluorescence intensity from the bonded pyranines monitors the weight average degree of polymerization and the growing gel fraction for below and above the gel point, respectively. This proportionality can easily be proven by using a Stauffer type argument under the assumption that the monomers occupy the sites of an imaginary periodic lattice [33, 34, 37].

Gelation theory often makes the assumption that the conversion factor,  $p$ , alone determines the behavior of the gelation process, though  $p$  may depend on temperature, concentration of monomers, and time [33, 37]. If the temperature and concentration are kept fixed, then  $p$  will be directly proportional to the reaction time,  $t$ . This proportionality is not linear over the whole range of reaction time, but



**Figure 3.** Fluorescence intensity of the free pyranine at 512 nm,  $I_{512\text{nm}}$ , versus reaction time for (a) 0.6% MWNTs, (b) 1% MWNTs and (c) 5% MWNTs content gel samples.

it can be assumed that in the critical region, i.e. around the critical point  $|p - p_c|$ , it is linearly proportional to  $|t - t_{\text{gel}}|$  [53, 54].

Therefore, below the gel point, i.e., for  $t < t_{\text{gel}}$ , the maximum fluorescence intensity,  $I'$ , measures the weight average degree of polymers (or average cluster size). Above  $t_{\text{gel}}$ , if the intensity from finite clusters distributed through the infinite network  $I_{\text{ct}}$  is subtracted from the maximum fluorescence intensity, then the corrected intensity  $I' - I_{\text{ct}}$  measures solely the gel fraction  $G$ , the fraction of the monomers that belong to the macroscopic network. In summary, we have the following relations [50],

$$I' \propto DP_w = C^+(t_{\text{gel}} - t)^{-\gamma}, \quad t \rightarrow t_{\text{gel}}^- \quad (8a)$$

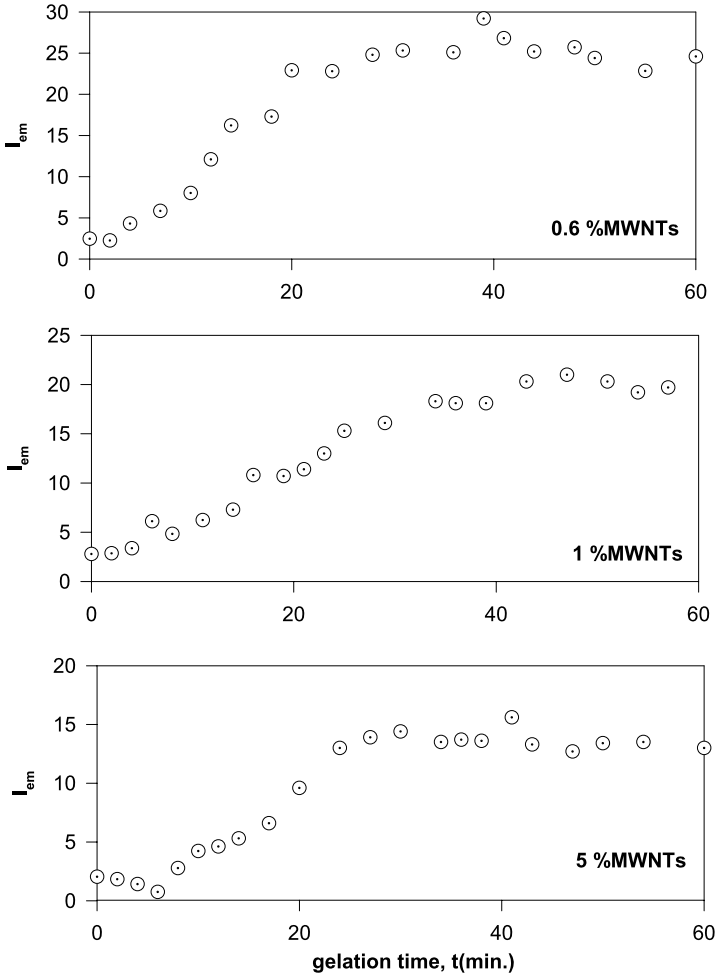


**Figure 4.** Variation of fluorescence intensity of pyranine at 427 nm, bonded to the PAM for different MWNT concentrations, versus reaction time for (a) 0.6% MWNTs, (b) 1% MWNTs and (c) 5% MWNTs contents.

$$I_{ct} \propto DP_w = C^-(t_{gel} - t)^{-\gamma'}, \quad t \rightarrow t_{gel}^+, \tag{8b}$$

$$I' - I_{ct} \propto G = B(t - t_{gel})^\beta, \quad t \rightarrow t_{gel}^+, \tag{9}$$

where  $C^+$ ,  $C^-$  and  $B$  are the critical amplitudes.

It is well known that the average cluster size of the finite clusters (distributed through the infinite network) above the gel point decreases with the same, but there is a negative slope to the increasing cluster size before the gel point. This means that the exponents  $\gamma$  and  $\gamma'$ , defined for the cluster sizes below and above the gel point, have the same values [33–37]. But, the critical amplitudes for the average cluster size defined below ( $C^+$  in equation 8(a)) and above ( $C^-$  in equation 8(b))

**Table 2.**  
Experimentally measured parameters for PAM–MWNTs composite gels

AAM (%)	MWNTs (%)	$t_{\text{gel}}$ (s)	$C^-/C^+$	$\beta$	$r$
100	0	$300 \pm 5$	1.0	0.92	–
			0.37	0.50	
			0.28	0.55	
			0.23	0.52	
			0.1	0.52	
99.9	0.1	$300 \pm 5$	1.0	0.75	$0.10 \pm 0.02$
			0.37	0.50	
			0.28	0.56	
			0.23	0.48	
			0.1	0.50	
99.8	0.2	$300 \pm 5$	1.0	1.05	$0.57 \pm 0.02$
			0.37	0.50	
			0.28	0.65	
			0.23	0.60	
			0.1	0.50	
99.7	0.3	$300 \pm 5$	1.0	0.75	$0.34 \pm 0.02$
			0.37	0.66	
			0.28	0.58	
			0.23	0.55	
			0.1	0.50	
99.4	0.6	$360 \pm 5$	1.0	0.96	$1.80 \pm 0.02$
			0.37	0.67	
			0.28	0.60	
			0.23	0.55	
			0.1	0.55	
99	1	$420 \pm 5$	1.0	0.90	$1.90 \pm 0.02$
			0.37	0.65	
			0.28	0.57	
			0.23	0.65	
			0.1	0.60	
97	3	$420 \pm 5$	1.0	0.83	$1.90 \pm 0.02$
			0.37	0.51	
			0.28	0.48	
			0.23	0.50	
			0.1	0.50	
95	5	$480 \pm 5$	1.0	1.10	$2.30 \pm 0.08$
			0.37	0.70	
			0.28	0.63	
			0.23	0.68	
			0.1	0.65	

**Table 2.**  
(Continued.)

AAm (%)	MWNTs (%)	$t_{gel}$ (s)	$C^-/C^+$	$\beta$	$r$
90	10	$540 \pm 5$	1.0	0.88	$1.80 \pm 0.05$
			0.37	0.72	
			0.28	0.57	
			0.23	0.60	
			0.1	0.56	
85	15	$660 \pm 5$	1.0	1.10	$1.90 \pm 0.02$
			0.37	0.45	
			0.28	0.40	
			0.23	0.41	
			0.1	0.40	

**Table 3.**  
The estimated values for the ratio  $C^-/C^+$  (from Ref. [55])

	Classical	Percolation			
		Direct $\varepsilon$ expansion	$\gamma_{\varepsilon exp} = 1.840$ and $\beta_{\varepsilon exp} = 0.52$	$\gamma = 1.7$ and $\beta = 0.4$	Series and Montecarlo
$C^-/C^+$	1	1/2.7	1/3.5	1/4.3	1/10

the gel point are different, and there exists a universal value for the ratio  $C^+/C^-$ . This ratio is different for mean-field *versus* percolation, as discussed by Aharony [55] and Stauffer *et al.* [33]. The estimated values for  $C^+/C^-$  [33, 55] are given in Table 3.

To determine the intensity  $I_{ct}$  in equations (8(b)) and (9), we first choose the parts of the intensity–time curves up to the gel points, then the mirror symmetry  $I_{ms}$  of these parts according to the axis perpendicular to the time axis at the gel point were multiplied by the ratio  $C^-/C^+$ , so that  $I_{ct} = \frac{C^-}{C^+} I_{ms}$ . Thus,  $I_{ct}$  measures solely the intensity from the cluster above the gel point, and  $I' - I_{ct}$  measures the intensity from the gel fraction. This process is clarified explicitly in Fig. 5.

Using equation (9), and the values for  $t_{gel}$  summarized in Table 2 we calculated  $\beta$  exponents as a function of AAm and/or the MWNT contents. Figure 6 represents the log–log plots of the typical intensity–time data above the gel point, for 0.6% MWNT and 3% MWNT concentrations, respectively, where the slope produced  $\beta$  values which are listed in Table 2 for various PAM–MWNTs.

#### 4.2. Conductivity Exponents

Figure 7 shows the conductivity as a function of alternating current frequency for composite gels with different content of PAM and/or MWNTs. It is observed that

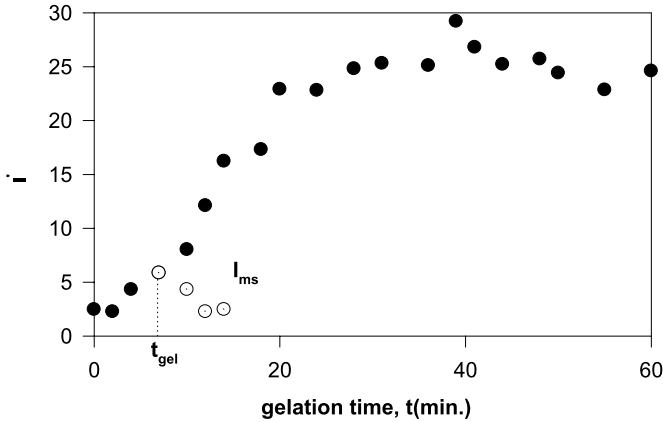


**Figure 5.** Intensity–time curve during formation of PAM–0.6% MWNTs composite gel. The curve depicted by dots represents the mirror symmetry  $I_{ms}$  of the intensity according to the axis perpendicular to time axis at  $t = t_{gel}$ . The intensity from the clusters above the gel point is calculated as  $I_{ct} = \frac{C^-}{C^+} I_{ms}$ .  $I' - I_{ct}$  monitors the growing gel fraction for  $t > t_{gel}$ . The intensity from the lower part of the symmetry axis monitors the average cluster size for  $t < t_{gel}$ .

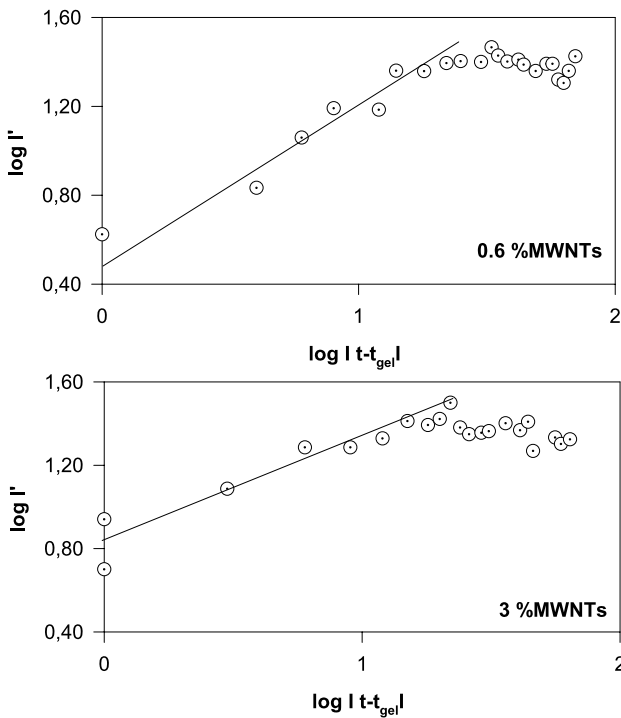


**Figure 6.** Double logarithmic plot of the intensity  $I'$  versus time curves above  $t_{gel}$  for 0.6% MWNTs and 3% MWNTs content gels, respectively. The  $\beta$  exponents are determined from the slope of the straight lines.

the conductivity behavior of the composite gels increases exponentially by increasing the AC frequency. The results show that the critical conductivity behavior of the composite system occurs at 4 kHz for lower MWNT contents while this behavior occurs at nearly 0 kHz for higher MWNT contents. PAM doped by the lower MWNT composite system converted into a conductive character at a higher frequency than the frequency value needed for PAM doped by a higher MWNT composite system. From Fig. 7, it may be seen that the conductivity, ( $\sigma$ ) of 0.3% MWNT gel was stable up to 4 kHz then suddenly increased to some point, and became stable. On the other hand, the conductivity, ( $\sigma$ ) for 1.0 and 3.0% MWNT gels increases suddenly at very low frequencies, then becomes stable after 4 kHz. It is observed that above the percolation threshold ( $>0.3$  wt%) and, after 4 kHz is reached, the conductivity becomes frequency independent. Such a phenomenon confirms the insulator to conductor transition at the critical concentration of conductive filler and/or above the percolation threshold the electrical properties of composites are dominated by the percolating paths of the conductive MWNTs.

Figure 8 shows the effect of MWNT contents on conductivity of PAM–MWNT composite gels at 5 kHz. At a very low content of MWNTs (0.3%), the conductiv-

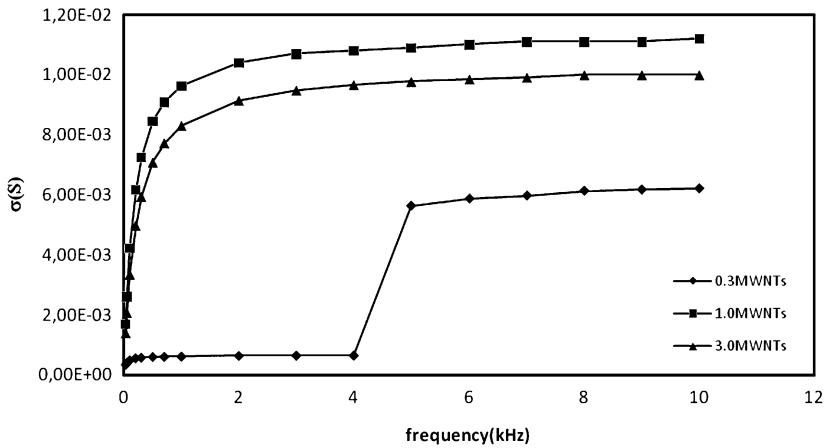


**Figure 7.** Conductivity of PAM–MWNTs composites *versus* alternating current (AC) frequency at room temperature for (a) 0.3% MWNTs, (b) 1.0% MWNTs and (c) 3.0% MWNTs content gel samples.

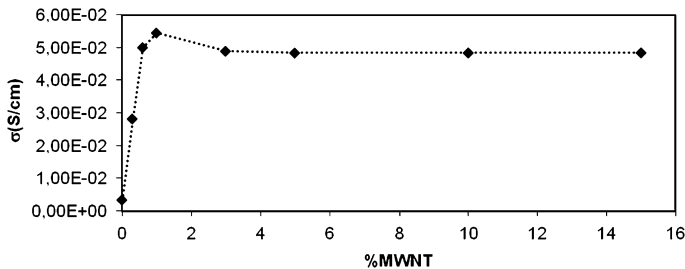


**Figure 8.** Conductivity as a function MWNTs content at 5 kHz frequency.

ity is quite low; however, after 0.3%, a definite increase in conductivity is observed. With this composition, the conductivity changes; in other words, whereas below this concentration the composites are resistant to electrical flow, above this value the composites are conductive. This stepwise change in conductivity is a result of the formation of an interconnected structure of MWNTs and can be regarded as an electrical percolation threshold, which simply means that at contents between 0.3 and 1.0% MWNTs, some percentage of electrons are permitted to flow through the specimen due to the creation of an interconnecting conductive pathway. At contents above 1.0% MWNTs, the conductivities are stable by increasing the MWNT content [29].

The value of the fitting exponent  $r$  in equation (7) was estimated from the slope of the linear relation between  $\log \sigma$  and  $\log w$  as shown in Fig. 9;  $s$  is the critical exponent which was taken from the literature as  $s \approx 0.7 \pm 0.05$ . The producer values are listed in Table 1 where it is seen that electrical percolation occurs above 0.3 wt% MWNTs with a critical exponent around  $r \approx 2$ , which is close to the theoretical prediction of this value in the 3D percolated system known as a random resistor network [44, 49].

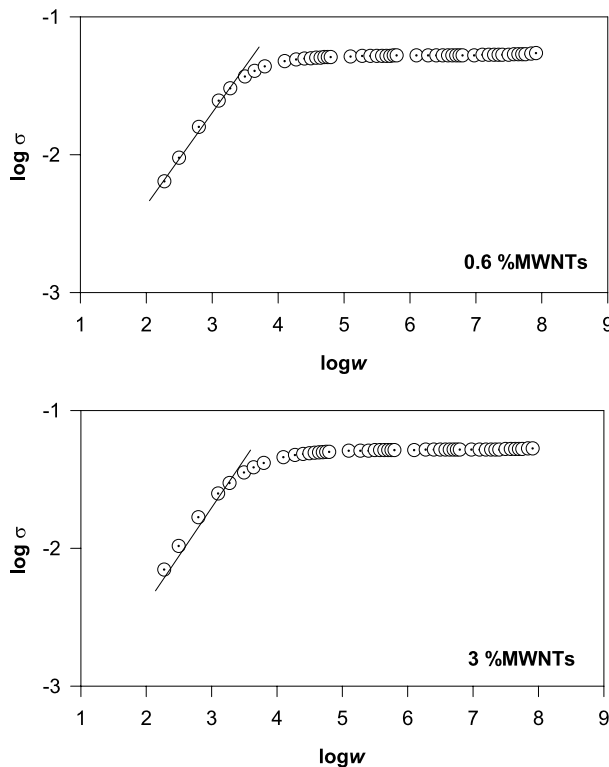


**Figure 9.** Logarithmic plot of the conductivity *versus* frequency curves of (a) 0.6% MWNTs and (b) 3% MWNTs content gel samples respectively.

## 5. Conclusion

In this work, we have been able to test the critical phenomena of the gelation and conductivity as a function of MWNT concentrations. It was found that the gel fraction exponent  $\beta$  obeyed the percolation theory for PAM–MWNT composite gels. It was also shown that if polymer systems which are initially of an isolator character are doped with carbon nanotubes of nano dimensions and when the amount of this addition exceeds a critical value known as the percolation threshold, then composite gel systems with carbon nanotubes added become electrically conducting structures.

The electrical percolation threshold occurs above 0.3% MWNTs with the critical exponent of  $r = 1.8$ – $2.3$  which is close to the theoretical prediction of this value in a 3D percolated system ( $r = 2$ ). The percolation critical exponent  $r$  obtained from fitting the composition dependence of the AC conductivity above the percolation threshold is consistent with the suggestions of percolation for a random resistor network.

Our future plan is to examine whether the critical conductivity exponent is identical for different polymer systems or not; in other words, whether it matches with a principle of universality which remains unstudied to date and is quite important for this area of study.

## References

1. S. Iijima, Helical microtubules of graphitic carbon, *Nature* **354**, 56–58 (1991).
2. G. Hu, C. Zhao, S. Zhang, M. Yang and Z. Wang, Low percolation thresholds of electrical conductivity and rheology in poly(ethylene terephthalate) through the networks of multi-walled carbon nanotubes, *Polymer* **47**, 480–488 (2006).
3. T.-E. Chang, A. Kisliuk, S. M. Rhodes, W. J. Britain and A. P. Sokolov, Conductivity and mechanical properties of well-dispersed single wall carbon nanotube/polystyrene composite, *Polymer* **47**, 7740–7746 (2006).
4. E. T. Thostenson, Z. F. Ren and T. W. Chou, Advances in the science and technology of carbon nanotubes and their composites: a review, *Compos. Sci. Technol.* **61**, 1899–1912 (2001).
5. K. T. Lau and D. Hui, The revolutionary creation of new advanced materials–carbon nanotube composites, *Composites, Part B: Engng* **33**, 263–277 (2002).
6. P. M. Ajayan, O. Stephan, C. Colliex and D. Trauth, Aligned carbon nanotube arrays formed by cutting a polymer resin nanotube composite, *Science* **265**, 1212–1214 (1994).
7. M. Moniruzzaman and K. I. Winey, Polymer nanocomposites containing carbon nanotubes, *Macromolecules* **39**, 5194–5205 (2006).
8. L. Gao, X. Zhou and Y. Ding, Effective thermal and electrical conductivity of carbon nanotube composites, *Chem. Phys. Letts* **434**, 297–300 (2007).
9. C. S. Choi, B. J. Park and H. J. Choi, Electrical and rheological characteristics of poly(vinyl acetate)/multi-walled carbon nanotube nanocomposites, *Diamond Rel. Mater.* **16**, 1170–1173 (2007).
10. F. Du, R. C. Scogna, W. Zhou, S. Brand, J. E. Fischer and K. I. Winey, Nanotube networks in polymer nanocomposites: rheology and electrical conductivity, *Macromolecules* **37**, 9048–9055 (2004).

11. S. J. Park, S. T. Lim, M. S. Cho, H. M. Kim, J. Joo and H. J. Choi, Electrical properties of multi-walled carbon-nanotube/poly(methyl methacrylate) nanocomposite, *Curr. Appl. Phys.* **5**, 302–304 (2005).
12. K. Anazawa, K. Shimotani, C. Manabe, H. Watanabe and M. Shimizu, High-purity carbon nanotubes synthesis method by an arc discharging in magnetic field, *Appl. Phys. Letts* **81**, 739–741 (2002).
13. Y. Bin, M. Mine, A. Koganemaru, X. Jiang and M. Matsuo, Morphology and mechanical and electrical properties of oriented PVA–VGCF and PVA–MWNT composites, *Polymer* **47**, 1308–1317 (2006).
14. E. Kymakis, I. Alexandou and G. A. J. Amaratunga, Single-walled carbon nanotube–polymer composites: electrical, optical and structural investigation, *Synthetic Metals* **127**, 59–62 (2002).
15. G. B. Blanchet, C. R. Fincher and F. Gao, Polyaniline nanotube composites: a high-resolution printable conductor, *Appl. Phys. Letts* **82**, 1290–1292 (2003).
16. M. S. P. Shaffer and A. H. Windle, Fabrication and characterization of carbon nanotube/poly(vinyl alcohol) composites, *Adv. Mater.* **11**, 937–941 (1999).
17. D. E. Hill, Y. Lin, A. M. Rao, L. F. Allard and Y.-P. Sun, Functionalization of carbon nanotubes with polystyrene, *Macromolecules* **35**, 9466–9471 (2002).
18. D. Qian, E. C. Dickey, R. Andrews and T. Rantell, Load transfer and deformation mechanisms in carbon nanotube–polystyrene composites, *Appl. Phys. Letts* **76**, 2868–2870 (2000).
19. R. Andrews, D. Jacques, D. Qian and T. Rantell, Multiwall carbon nanotubes: synthesis and application, *Acc. Chem. Res.* **35**, 1008–1017 (2002).
20. T. Tanaka, *Gels, Sci. Amer.* **244**, 110–124 (1981).
21. G. M. Barrow, *Introduction to Molecular Spectroscopy*. McGraw-Hill, New York, NY, USA (1962).
22. J. B. Birks, *Photophysics of Aromatic Molecules*. Wiley Interscience, London, UK (1970).
23. D. M. Hercules, *Fluorescence and Phosphorescence Analysis*. Wiley Interscience, New York, NY, USA (1965).
24. M. D. Galanin, *Luminescence of Molecules and Crystals*. Cambridge International Science Publishing, Cambridge, UK (1995).
25. P. Pötschke, M. Abdel-Goad, I. Alig, S. Dudkin and D. Lellinger, Rheological and dielectrical characterization of melt mixed polycarbonate-multiwalled carbon nanotube composites, *Polymer* **45**, 8863–8870 (2004).
26. S. Barrau, P. Demont, A. Peigney, C. Laurent and C. Lacabanne, DC and AC conductivity of carbon nanotubes–polyepoxy composites, *Macromolecules* **36**, 5187–5194 (2003).
27. M. Weber and M. R. Kamal, Estimation of the volume resistivity of electrically conductive composites, *Polym. Compos.* **18**, 711–725 (1997).
28. P. Pötschke, S. M. Dudkin and I. Alig, Dielectric spectroscopy on melt processed polycarbonate-multiwalled carbon nanotube composites, *Polymer* **44**, 5023–5030 (2003).
29. M.-K. Seo and S.-J. Park, Electrical resistivity and rheological behaviors of carbon nanotubes-filled polypropylene composites, *Chem. Phys. Letts* **395**, 44–48 (2004).
30. X. Li, W. Guan, H. Yan and L. Huang, Fabrication and atomic force microscopy/friction force microscopy (AFM/FFM) studies of polyacrylamide–carbon nanotubes (PAM–CNTs) copolymer thin films, *Mater. Chem. Phys.* **88**, 53–58 (2004).
31. P. J. Flory, Molecular size distribution in three-dimensional polymers. I. Gelation, *J. Amer. Chem. Soc.* **63**, 3083–3090 (1941).
32. W. H. Stockmayer, Theory of molecular size distribution and gel formation in branched-chain polymers, *J. Chem. Phys.* **11**, 45–54 (1943).

33. D. Stauffer, A. Coniglio and M. Adam, Gelation and critical phenomena, *Adv. Polym. Sci.* **44**, 103–158 (1982).
34. D. Stauffer, *Introduction to Percolation Theory*. Taylor and Francis, London, UK (1985).
35. P. G. de Gennes, *Scaling Concepts in Polymer Physics*. Cornell University Press, Ithaca, NY, USA (1988).
36. H. J. Herrmann, Geometrical cluster growth models and kinetic gelation, *Phys. Rep.* **136**, 153–224 (1986).
37. D. Stauffer and A. Aharony, *Introduction to Percolation Theory*, 2nd edn. Taylor and Francis, London, UK (second printing) (1994).
38. M. Gordon, Good's theory of cascade processes applied to the statistics of polymer distributions, *Proc. Royal Soc., London A* **268**, 240–256 (1962).
39. C. W. Macosko and D. R. Miller, A new derivation of average molecular weights of nonlinear polymers, *Macromolecules* **9**, 199–206 (1976).
40. D. S. Pearson and W. W. Graessley, The structure of rubber networks with multifunctional junctions, *Macromolecules* **11**, 528–533 (1978).
41. D. Durand and C.-M. Bruneau, Reactivity and gelation. I. Intrinsic reactivity, *J. Polym. Sci. Polym. Phys. Ed.* **17**, 273–294 (1979).
42. D. J. Bergman and Y. Imry, Critical behavior of the complex dielectric constant near the percolation threshold of a heterogeneous material, *Phys. Rev. Letts* **39**, 1222–1225 (1977).
43. M. Sahimi, *Application of Percolation Theory*. Taylor and Francis, London, UK (1994).
44. J. P. Straley, Critical exponents of conductivity of random resistor lattices, *Phys. Rev. B* **15**, 5733–5737 (1977).
45. R. Fisch and A. B. Harris, Critical behavior of random resistor networks near the percolation threshold, *Phys. Rev. B* **18**, 416–420 (1978).
46. J. Adler, Y. Meir, A. Aharony, A. B. Harris and L. Klein, Low-concentration series in general dimension, *J. Stat. Phys.* **58**, 511–538 (1990).
47. D. B. Gingold and C. J. Lobb, Percolative conduction in three dimensions, *Phys. Rev. B* **42**, 8220–8224 (1990).
48. H. J. Herrman, B. Derrida and J. Vannimenus, Superconductivity exponents in two and three dimensional percolation, *Phys. Rev. B* **30**, 4080–4082 (1984).
49. B. Derrida, D. Stauffer, H. J. Herrman and J. Vannimenus, Transfer matrix calculation of conductivity in three-dimensional random resistor networks at percolation threshold, *Le J. de Phys. Letts* **44**, L701–L706 (1983).
50. D. Kaya, Ö. Pekcan and Y. Yılmaz, Direct test of the critical exponents at the sol–gel transition, *Phys. Rev. E* **69**, 16117 (1–10) (2004).
51. Y. Yılmaz, N. Uysal, A. Gelir, O. Guney, D. K. Aktaş, S. Gogebakan and A. Oner, Elucidation of multiple-point interactions of pyranine fluoroprobe during the gelation, *Spectrochimica Acta Part A: Mol. Biomolecular Spect.* **72**, 332–338 (2009).
52. O. Okay, D. Kaya and Ö. Pekcan, Free-radical crosslinking copolymerization of styrene and divinylbenzene: real time monitoring of the gel effect using fluorescence probe, *Polymer* **40**, 6179–6187 (1999).
53. Y. Yılmaz, A. Erzan and Ö. Pekcan, Critical exponents and fractal dimension at the sol–gel phase transition *via in situ* fluorescence experiments, *Phys. Rev. E* **58**, 7487–7491 (1998).
54. Y. Yılmaz, A. Erzan and Ö. Pekcan, Slow release percolate near glass transition, *Eur. Phys. J. E* **9**, 135–141 (2002).
55. A. Aharony, Universal critical amplitude ratios for percolation, *Phys. Rev. B* **22**, 400–414 (1980).